OPEN ACCESS

Microbiology ARTICLE

Structural insights into the functional convergence of two divergent cytochrome P450 enzymes

Li Ma,[1,6] Sheng Dong,[2,4,5,6] Jiashuai Zhang,[1] Mingyu Liu,[1] Yuxuan Li,[1] Xisong Feng,[1] Haibo Zhang,[2,4,5] Wei Peng,[1,*] Yingang Feng,[2,4,5,*] and Shengying Li[1,3,*]

*Correspondence: weipeng@sdu.edu.cn (W.P.); fengyg@qibebt.ac.cn (Y.F.); lishengying@sdu.edu.cn (S.L.)

Received: December 26, 2025; Accepted: May 20, 2026; Published Online: May 27, 2026; https://doi.org/10.59717/j.xinn-life.2026.100221

GRAPHICAL ABSTRACT

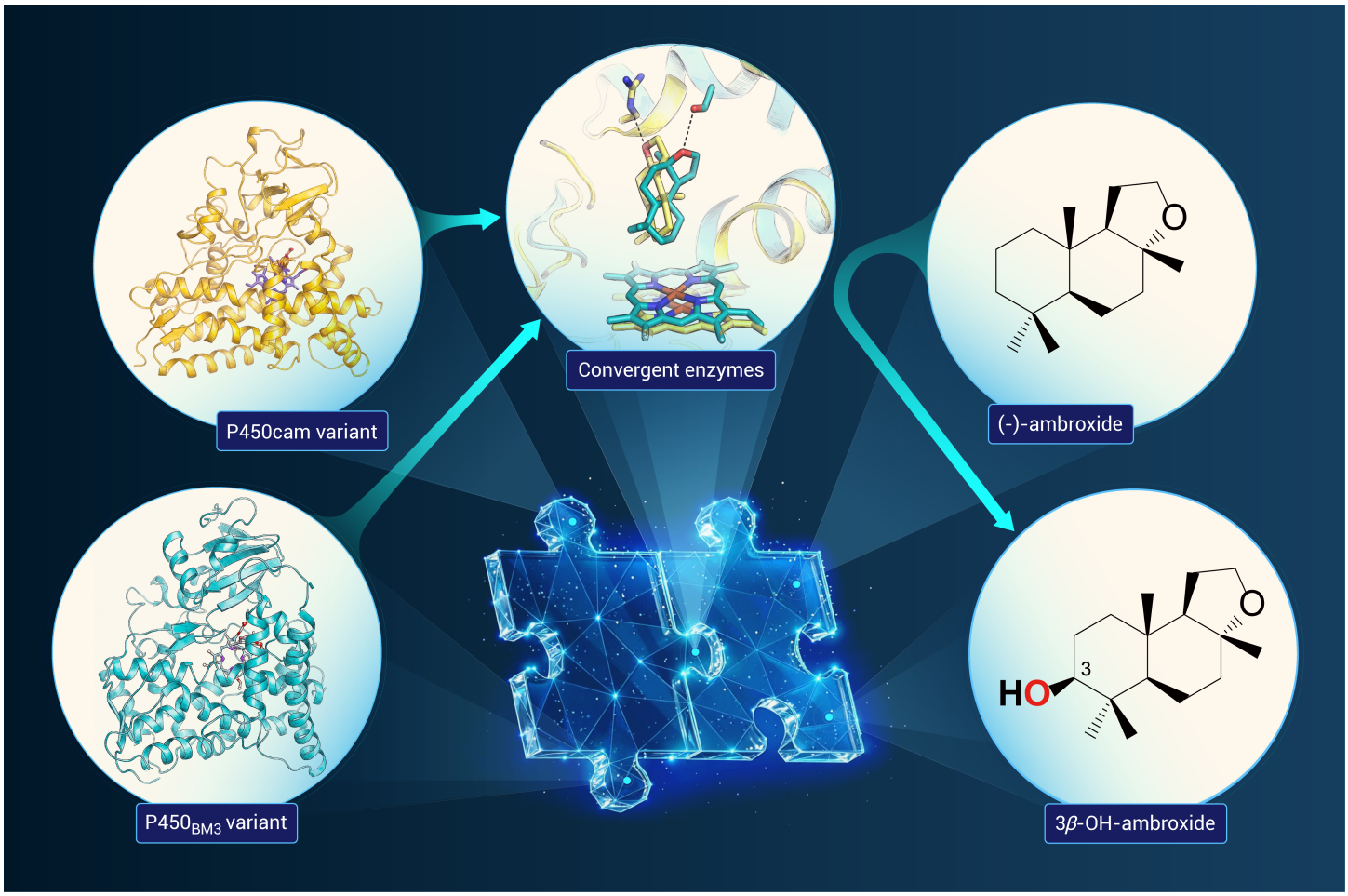

PUBLIC SUMMARY

- Cytochrome P450 enzymes are powerful biocatalysts for selective C–H bond oxidation.
- Functional convergence of divergent P450s enable regio- and stereoselective oxidation of the same substrate.
- Catalytic pocket geometry and polar residues govern P450 substrate orientation and catalytic selectivity.

ARTICLE Microbiology

OPEN ACCESS

www.the-innovation.org/the-innovation-life

Structural insights into the functional convergence of two divergent cytochrome P450 enzymes

Li Ma,[1,6] Sheng Dong,[2,4,5,6] Jiashuai Zhang,[1] Mingyu Liu,[1] Yuxuan Li,[1] Xisong Feng,[1] Haibo Zhang,[2,4,5] Wei Peng,[1,*] Yingang Feng,[2,4,5,*] and Shengying Li[1,3,*]

[1]State Key Laboratory of Microbial Technology, Shandong University, Qingdao 266237, China

[2]Qingdao Institute of Bioenergy and Bioprocess Technology, Chinese Academy of Sciences, Qingdao 266237, China

[3]Laboratory for Marine Biology and Biotechnology, Qingdao Marine Science and Technology Center, Qingdao 266237, China

[4]Shandong Energy Institute, Qingdao New Energy Shandong Laboratory, Qingdao 266101, China

[5]University of Chinese Academy of Sciences, Beijing 100049, China

[6]These authors contributed equally

*Correspondence: weipeng@sdu.edu.cn (W.P.); fengyg@qibebt.ac.cn (Y.F.); lishengying@sdu.edu.cn (S.L.)

Received: December 26, 2025; Accepted: May 20, 2026; Published Online: May 27, 2026; https://doi.org/10.59717/j.xinn-life.2026.100221

Citation: Ma L., Dong S., Zhang J., et al. (2026). Structural insights into the functional convergence of two divergent cytochrome P450 enzymes. *The Innovation Life* **4**:100221.

Cytochrome P450 enzymes are versatile biocatalysts for a broad spectrum of oxidative reactions and a hotspot for protein engineering. Using the "multi-enzymes-for-multi-substrates" directed evolution strategy, we have found a number of mutants of the two archetypal P450 enzymes (*i.e.*, P450cam and $P450_{BM3}$) to catalyze the regio- and stereoselective oxidation of the perfume compound (−)-ambroxide. Despite their low sequence similarity, these mutant enzymes exhibit a convergent activity of 3β-hydroxylation as a result of laboratory-directed evolution. To address the longstanding interest in elucidating the principle underlying substrate recognition and catalytic specificity of P450 enzymes, herein, we resolve the crystal structures of P450cam-F87R and $P450_{BM3}$-F87A/L75N/V78S (heme domain) in complex with (−)-ambroxide. Comparative analysis reveals how specific amino acid mutations reshape the substrate-binding pocket, thereby enhancing substrate accommodation and catalytic precision. The introduction of polar residues in the catalytic pocket is essential for controlling the optimal orientation of the substrate with a heterocycle. These findings underscore the importance of the pocket shape and polarity in enzyme redesign and provide valuable insights for the (semi-)rational engineering of P450 enzymes.

INTRODUCTION

Selective oxidation of inert C−H bonds is an effective means for rapid construction and late-stage modification of diverse organic molecules, thus endowing the products with desired physiochemical, biological, and pharmaceutical properties.[1] Despite a growing number of promising advances,[2-6] it remains challenging in the field of chemical synthesis to achieve highly regio- and stereoselective oxofunctionalization of complex compounds containing multiple C−H bonds with similar reactive properties (*e.g.*, natural products with multiple chiral centers including terpenoids, polyketides, and non-ribosomal peptides[7,8]).

In nature, the superfamily of cytochrome P450 enzymes (CYPs or P450s) possess unique abilities to selectively oxidize inert C−H bonds in countless natural and man-made compounds. These versatile enzymes have shown the broadest substrate scope and reaction diversity in nature.[9-11] Thus, these heme-thiolate proteins offer an attractive biocatalytic option for both biological and chemical syntheses. Despite the highly diversified sequences of more than one million discovered P450 family members, all resolved and predicted CYP proteins share a conserved three-dimensional structure and possess an absolutely conserved cysteine residue as the proximal ligand and a water molecule as the distal ligand in the resting state, which are both linked to the heme-iron catalytic center.[12] In the well-known catalytic cycle, the binding of substrate displaces the distal ligand and initiates the electron transfer from NAD(P)H to heme-iron via redox partner protein(s), which in turn activates dioxygen for selective oxidation.[13] Although P450s maintain such conserved structural features and catalytic cycle, they exhibit remarkable diversity in substrate specificity, and reaction types and selectivity. This contradiction raises a fundamental question: what structural and/or dynamic factors govern their vastly different substrate preferences and catalytic outcomes?

To date, only a few bacterial P450s have been characterized in sufficient detail to serve as paradigms for understanding the catalytic mechanisms of P450 enzymes, most notably P450cam (CYP101A1) and $P450_{BM3}$ (CYP102A1). Both enzymes have been intensively studied for decades, providing fundamental insights into the structural and mechanistic principles of P450 catalysis while also serving as model systems for protein engineering.[14,15] As a result, these two enzymes have been heavily engineered to catalyze a large variety of unnatural reactions, many of which are scientifically groundbreaking or industrially relevant. Specifically, P450cam from *Pseudomonas putida* catalyzes the regio- and stereoselective hydroxylation of (+)-camphor to 5-*exo*-hydroxycamphor, when supported by its native redox partners putidaredoxin (Pdx) and putidaredoxin reductase (PdR).[16] As the first P450 structure solved, P450cam has long been central to understanding the catalytic cycle, substrate recognition, and structure-function relationship.[15,17-20] $P450_{BM3}$ from *Bacillus megaterium* naturally fuses a P450 domain (also termed heme domain) with a eukaryotic-like diflavin reductase domain, which was initially characterized for its superb catalytic activity toward long-chain fatty acids.[21] Continuous rational redesign and extensive directed evolution efforts have transformed $P450_{BM3}$ into a leading platform for P450-based biocatalysis, biotransformation, and even drug development since the engineered variants are capable of oxidizing a wide range of substances, including pharmaceuticals, synthetic precursors, flavors, fragrances, and pheromones.[14]

Nonetheless, these two classical P450 enzymes have largely been studied with a focus on their individual functions, mechanisms, and engineering, without systematic comparative analysis across P450cam and $P450_{BM3}$ with regard to their substrate recognition and catalytic selectivity. Notably, P450cam and $P450_{BM3}$ share only a 17.2% sequence identity and exhibit a root-mean-square deviation (RMSD) of 11.67 Å in their three-dimensional structures, underscoring their distant evolutionary relationship.[22] In our previous study, we established a "multi-enzymes-for-multi-substrates" (MEMS) directed evolution model by co-evolving P450cam and $P450_{BM3}$ towards seven selected substrates. This throughput-multiplied approach enabled the observation of a series of convergent evolution events of the two prototypic P450s arising from laboratory-directed evolution. In particular, the isoenzymes, including P450cam-F87R and several $P450_{BM3}$ mutants, share the ability to selectively catalyze the 3β-hydroxylation of (−)-ambroxide (a high-value commercial fragrance) to form 3β-OH-ambroxide (with a delightful aroma distinct from that of (−)-ambroxide). Thus, it is mechanistically intriguing to understand how these two distinct P450 active sites converge on the same catalytic function.

In this study, we determined the crystal structures of P450cam-F87R and $P450_{BM3}$-F87A/L75N/V78S (heme domain) in complex with (−)-ambroxide, facilitating direct structural comparisons to understand the structure-function relationship and to further alter the regioselectivity of P450 biocatalysts by fine-tuning the enzyme active pocket. The structural and biochemical analyses of the two selected isoenzymes provide not only new insights into the mechanisms of P450 substrate binding/orientation, but also rational guidance for designing mutants to target new specific substrates and reactions.

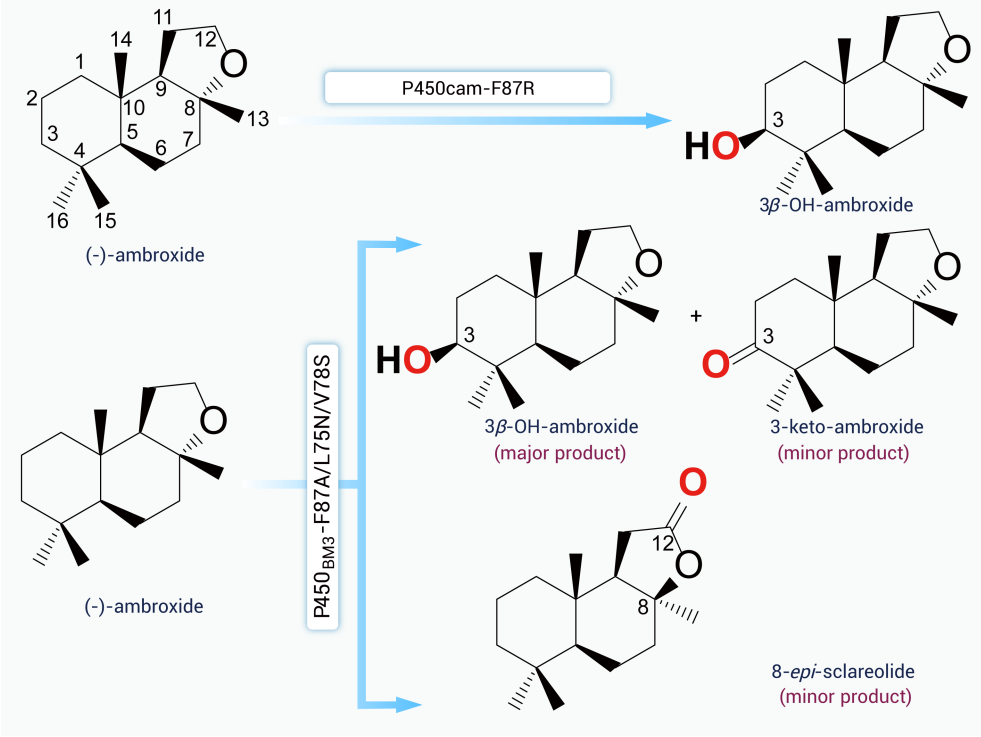

Figure 1. Schematic oxidative reactions of (−)-ambroxide The reaction pathways illustrate that P450cam and $P450_{BM3}$ variants exhibit convergent 3β-hydroxylation activity.

MATERIALS AND METHODS

Materials

Antibiotics and chemicals were obtained from SolarBio (Beijing, China) and Sigma-Aldrich (St. Louis, MO, USA), respectively. The I-5™ 2× High-Fidelity Master Mix was purchased from Tsingke Biological Technology (Beijing, China). Plasmid extraction and DNA purification kits were purchased from Qingdao Baisai Biotechnology. For His-tagged protein purification, Sangon Biotech Ni-NTA Sefinose™ Resin (Settled Resin) (Shanghai, China) was utilized. Millipore Amicon Ultra centrifugal filters (Billerica, MA, USA) and PD-10 desalting columns from GE Healthcare (Piscataway, NJ, USA) were employed. Oligonucleotide synthesis and DNA sequencing services were provided by Sangon Biotech (Shanghai, China).

Analysis procedures

The UV-visible spectra were obtained using a Spectrophotometer Infinite M200 Pro (Tecan Group Ltd., Switzerland). GC and GC-MS analyses were conducted on Agilent 7890B and 1200 series instruments (Agilent Technologies Inc., Santa Clara, USA) equipped with an Agilent HP-5 column (30 m × 0.32 mm, 0.25 μm). GC analysis was performed with the following program: the temperature was increased from 50°C to 260°C at a rate of 10°C min^{-1}, and held at 260°C for 8 min. HRESI-MS data were acquired using a maXis ultra-high-resolution TOF system (Bruker Daltonik, Germany). Masses of negatively charged ions were calibrated with aqueous sodium formate as an internal standard. Reaction samples were analyzed by HPLC/HRMS using a Triart C18 column (5 μm, 4.6 mm × 250 mm, YMC Co., Ltd., Japan). Separation of 8-*epi*-sclareolide was carried out under gradient elution with two solvent systems: solvent A (water with 0.1% *v*/*v* TFA) and solvent B (acetonitrile with 0.1% *v*/*v* TFA). The gradient profile was as follow: 0-17 min, 70% solvent B; 17-24 min, 70-100% solvent B; 24-26 min, 70% solvent B. Detection was performed at 254 nm with a flow rate of 1 mL/min. Nuclear magnetic resonance (NMR) spectra were acquired on a Bruker 600 MHz spectrometer (Bruker BioSpin GmbH Co., Rheinstetten, Germany). All NMR data were processed using MestReNova software.

Protein expression and purification

For heterologous expression, the target genes P450cam-F87R and $P450_{BM3}$-F87A/L75N/V78S were individually cloned into the pET30a expression vector and transformed into *Escherichia coli* BL21(DE3) cells. A single colony of the transformant was selected and inoculated into the LB medium supplemented with 50 mg/L kanamycin. The overnight seed culture was used for a 1:100 inoculation of 0.5 L TB medium containing 50 mg/L kanamycin, 1 mM thiamin, and the rare salt solution. The *E. coli* cells were incubated at 37°C for 2-3 h until OD_{600} reached 0.4-0.6. Subsequently, IPTG was added to achieve a final concentration of 0.2 mM to induce gene expression, and 0.5 mM 5-aminolevulinic acid was supplemented as a precursor for heme synthesis. The cells were then cultured at 20°C for another 20 h. The culture was subjected to centrifugation at 6,000 × *g* for 10 min to pellet cells. Protein purification was subsequently performed according to a previously established procedure.[23,24] The purified proteins were flash-frozen in liquid nitrogen and stored at −80°C for future use. P450cam and $P450_{BM3}$ were purified following the methods outlined in prior studies.[25,26] The functional concentrations of P450 were determined using CO-reduced difference spectra, employing an extinction coefficient of $\varepsilon_{450-490}$ = 91,000 M^{-1} cm^{-1}.[27] However, the $P450_{BM3}$-F87A/L75N/V78S mutant exhibited a maximum absorption of the Fe^{2+}–CO complex at around 420 nm (Figure S1). The altered spectroscopic feature did not eliminate the activity of this mutant. The protein concentration was determined using an extinction coefficient of ε_{420} nm = 110,000 M^{-1} cm^{-1} for the P420 form of the protein.[28] The concentrations of ferredoxin and ferredoxin reductase were determined by measuring the absorbance at selected wavelengths. The extinction coefficients used for these calculations were ε_{420} = 10,200 M^{-1}·cm^{-1} for Pdx and ε_{455} = 10,400 M^{-1}·cm^{-1} for PdR.[29]

Activity analysis

Reactions of P450 mutants were performed according to the previous report.[22] The standard assay contained 2 μM P450, 1 mM NADPH/NADH, and 0.5 mM substrate in 100 μL potassium phosphate buffer (pH 7.4) was incubated at 30°C for 2 h. For P450cam, 2 μM Pdx and 2 μM PdR were needed. To quench the reaction, 100 μL ethyl acetate was added to the reaction mixture. After thorough vortex mixing and high-speed centrifugation (12,000 × *g*, 15 min), the supernatant was subjected to GC analysis.

Determination of substrate affinity

The binding affinity of the substrate (−)-ambroxide to both the wild-type and mutant P450cam and $P450_{BM3}$ (heme domain) was quantified by determining the dissociation constants (K_D).[30] This was achieved through the application of UV-visible absorption titrations. The experiment was conducted with 1 μM of P450 protein in a 50 mM potassium phosphate buffer at pH 7.4. The measurements were taken in a quartz cuvette with a 1-cm path length. Spectra were recorded during the substrate titrations, and the overall change values ΔA (A_{peak} - A_{trough}) were plotted against the substrate concentrations. Data were plotted and fitted to the hyperbolic function $\Delta A = Amax\ S / (K_D + S)$, where S is the total substrate concentration, $Amax$ is the maximal absorption shift at saturation, and K_D is the apparent dissociation constant of the enzyme-substrate complex.

Steady-state kinetics

The kinetic assays were conducted using gas chromatography (GC) and were based on at least three independent measurements. In a standard experiment, the concentration of (−)-ambroxide ranged from 0.1 to 2.5 mM. The P450 enzyme was added in an appropriate concentration to ensure that substrate consumption remained within a linear range. All necessary cofactors were added in excess. The reactions were initiated by adding NADPH or

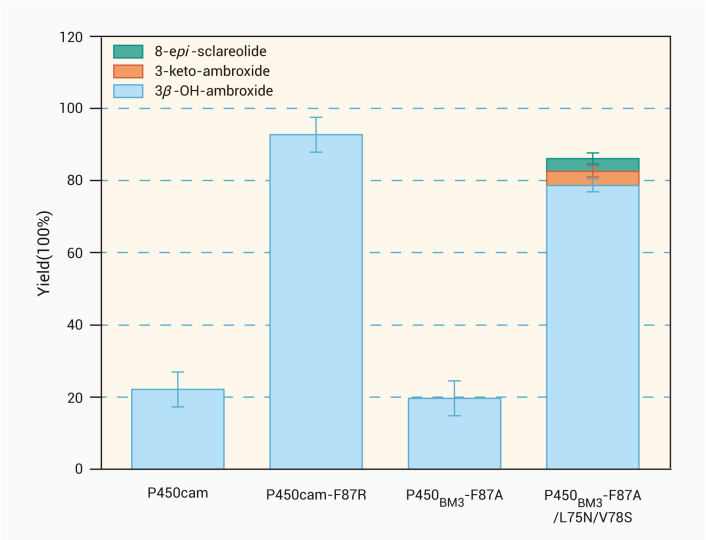

Figure 2. Product distribution of wild-type and mutant P450 enzymes Data are presented as mean ± SD from three independent replicates (n = 3). Error bars are shown in different colors for each product (3β-OH-ambroxide in blue, 3-keto-ambroxide in orange, and 8-*epi*-sclareolide in green).

NADH and were halted by thoroughly mixing with an equal volume of ethyl acetate at 0, 30 and 60 seconds. The k_{cat} and K_m values were determined by fitting the velocity data to the Michaelis-Menten equation.

Crystallization, data collection, and structure determination

The purified P450cam and $P450_{BM3}$ (heme domain) for crystallization were concentrated to approximately 20 mg/mL in 10 mM Tris-HCl (pH 8.0) and 100 mM NaCl. Crystals were obtained using the sitting-drop vapor diffusion method for initial screening and the hanging-drop vapor diffusion method for subsequent optimization, conducted at 18°C. In order to generate crystals of the target protein complex with (−)-ambroxide, P450cam-F87R and $P450_{BM3}$-F87A/L75N/V78S were mixed with (−)-ambroxide at a molar ratio of 1:20, respectively. High-quality crystals were obtained under the conditions shown in Table S1. All crystals utilized for data collection were cryoprotected by soaking in a well solution supplemented with 20% (*v*/*v*) glycerol for a duration of 10 seconds, followed by flash-cooling in liquid nitrogen. X-ray diffraction data were collected on the BL19U1 or BL10U2 at the Shanghai Synchrotron Radiation Facility (SSRF).[31,32] Data indexing, integration, and scaling were conducted using XDS.[33,34] The structures of P450cam-F87R and $P450_{BM3}$-F87A/L75N/V78S were determined by molecular replacement, employing the PHENIX program suite and using the PDB files 2A1M and 1ZO9 as the search models, respectively.[34,35] The refinement of the structure was performed using the COOT and PHENIX programs.[36,37] The data collection and refinement statistics are shown in Table S1. All molecular graphics were created with PyMOL (http://www.pymol.org).

RESULTS

Biochemical analysis of the (−)-ambroxide 3β-hydroxylases with different origins

Wild-type $P450_{BM3}$ shows no detectable catalytic activity toward (−)-ambroxide (Figure S2). In contrast, the F87A mutant of $P450_{BM3}$, which features an expanded active site and broadened substrate scope, exhibits weak but measurable activity and was therefore used as the starting enzyme. In our previous work, the co-directed evolution of P450cam and $P450_{BM3}$-F87A, despite their low sequence similarity and distinct substrate scopes, resulted in a common catalytic activity of 3β-hydroxylation of (−)-ambroxide (Figure 1). Specifically, the wild-type P450cam achieved 21.0 ± 5.1% conversion and produced only 3β-OH-ambroxide. In comparison, $P450_{BM3}$-F87A showed 18.9 ± 5.2% conversion and yielded 3β-OH-ambroxide as the main product with a minor amount of 12-keto product 8-*epi*-sclareolide as detected by LC-MS (Figures 2 & S2). Upon laboratory-directed co-evolution of P450cam and $P450_{BM3}$-F87A, the most regioselective mutants were identified to be P450cam-F87R and $P450_{BM3}$-F87A/L75N/V78S. Specifically, P450cam-F87R and $P450_{BM3}$-F87A/L75N/V78S converted 90.0 ± 4.3% and 85.5 ± 5.6% of substrate, respectively, achieving regioselectivity of 100% and 96.0% upon a 2-h reaction at 30 °C.

Compared to P450cam-F87R, $P450_{BM3}$-F87A/L75N/V78S has a considerably larger substrate binding pocket (Figure S3), which likely accounts for its lower regioselectivity toward (−)-ambroxide due to less steric constraint. As a result, the initially formed 3β-OH-ambroxide can rebind to the active site and undergo the second oxidation, producing 3-keto-ambroxide as a minor product. Interestingly, the triple mutant also yielded a small amount of 8-*epi*-sclareolide (Figures S4-S9). This C12-oxidized product indicates that the substrate could bind to the same active pocket in opposite orientations, thus alternatively presenting C-3 or C-12 C−H bond for oxidation.

Subsequently, we compared the substrate binding affinities of different P450 variants by measuring the spectral changes upon substrate titrations.[38] For P450cam-derived (−)-ambroxide 3β-hydroxylase, the substrate conversion ratio of P450cam-F87R was approximately threefold higher than that of P450cam-WT. The substrate dissociation constant (K_D) of P450cam-F87R was determined to be 87.3 ± 11.1 μM, only slightly lower than that of the wild-type enzyme (K_D = 91.1 ± 9.8 μM) (Table 1 & Figure S10). Thus, we further compared their steady-state kinetic parameters and the k_{cat}/K_m value of P450cam-F87R showed a 3.2-fold improvement relative to P450cam-WT. Collectively, the increased activity of P450cam-F87R likely resulted from the significantly enhanced k_{cat} (Table 1 & Figure S11). With regard to $P450_{BM3}$ mutants, $P450_{BM3}$-F87A/L75N/V78S exhibited higher substrate binding affinity towards (−)-ambroxide (K_D = 10.2 ± 0.1 μM) when compared to its parental enzyme $P450_{BM3}$-F87A (K_D = 230.1 ± 16.7 μM) (Table 1 & Figure S10). The catalytic efficiency (k_{cat}/K_m) was determined to be 2.39 $\mu M^{-1}\cdot min^{-1}$ (Table 1 & Figure S11), representing 2.5-fold improvement compared to that of $P450_{BM3}$-F87A (k_{cat}/K_m = 0.69 $\mu M^{-1}\cdot min^{-1}$).

Structural basis for the regio- and stereoselectivity of (−)-ambroxide 3β-hydroxylases

To understand the structural basis for the regio- and stereoselectivity of P450cam-F87R and $P450_{BM3}$-F87A/L75N/V78S as alternative (−)-ambroxide 3β-hydroxylases, we determined the crystal structures of substrate-free P450cam-F87R at 1.74 Å resolution (PDB ID: 25BV), the P450cam-F87R−(−)-ambroxide complex at 2.04 Å resolution (PDB ID: 9L7R), and the $P450_{BM3}$-F87A/L75N/V78S-(−)-ambroxide complex at 2.70 Å resolution (PDB ID: 9L7U; heme domain only), respectively (Table S1); the structure of the substrate-free $P450_{BM3}$-F87A/L75N/V78S was not obtained after several thorough screenings of crystallization conditions. The organization of secondary structural elements in these structures is conserved, as exemplified by the B/C loop, B' helix, F/G region, and β4-loop (Figure 3A, D, & S12). The F87R mutation in P450cam has a minimal impact on the overall protein structure, with an RMSD of approximately 0.327 Å upon superposition with the wild-type enzyme (PDB ID: 2A1M)[34] (Figure 3A). P450cam-F87R has a hydrophobic substrate binding pocket composed of Y96, F98, M184, F193, L244, V247, V295, I395, and V396 (Figure 3B). The F87R mutation within the B/C loop introduces a clear electron density and forms a hydrogen bond (2.5 Å) with the main chain oxygen of M184 in the F-helix (Figure 3C). This structural change increases the volume of the active pocket from 343 $Å^3$ to 401 $Å^3$ (a 17% increase) (Figure S3), thereby enabling the accommodation of a larger substrate, (−)-ambroxide ($C_{16}H_{28}O$), compared to the native substrate (+)-camphor ($C_{10}H_{16}O$).

The mutations F87A/L75N/V78S introduced into $P450_{BM3}$ also did not induce significant overall structural changes, with an RMSD of approximately 0.406 Å compared to the wild-type enzyme (PDB ID: 1ZO9) (Figure 3D). $P450_{BM3}$-F87A/L75N/V78S has a hydrophobic substrate binding pocket primarily composed of A74, L75, F81, A82, A87, L181, I263, A264, A328, and L437 (Figure 3E). The F87A substitution lies within the B/C loop, and the L75N and V78S mutations are positioned in the B'-helix (Figure 3F). The replacement of Leu75 with Asn allows the nitrogen atom of the side-chain amide group to form a hydrogen bond (2.8 Å) with the backbone oxygen of A87. These mutations remarkably expand the catalytic pocket, particularly through the structural changes induced by F87A, which increase the pocket volume from 564 $Å^3$ to 685 $Å^3$ (a 21% increase) (Figure S3). Of note, the F87A substitution has been widely utilized in engineering various $P450_{BM3}$ mutants.[39-42] In

Table 1. Kinetic parameters of P450cam and $P450_{BM3}$ variants toward (−)-ambroxide Data are presented as mean ± SD from three independent replicates (n = 3).

enzyme	K_D (μM)	K_m (μM)	k_{cat} (min^{-1})	k_{cat}/K_m ($μM^{-1}·min^{-1}$)
wild-type P450cam	91.1 ± 9.8	753.8 ± 129.2	230.3 ± 8.3	0.31
P450cam-F87R	87.3 ± 11.1	595.9 ± 87.5	778.9 ± 43.8	1.30
$P450_{BM3}$-F87A	230.1 ± 16.7	745.1 ± 151.7	513.3 ± 5.8	0.69
$P450_{BM3}$-F87A/L75N/V78S	10.2 ± 0.1	349.0 ± 19.8	834.1 ± 19.9	2.39

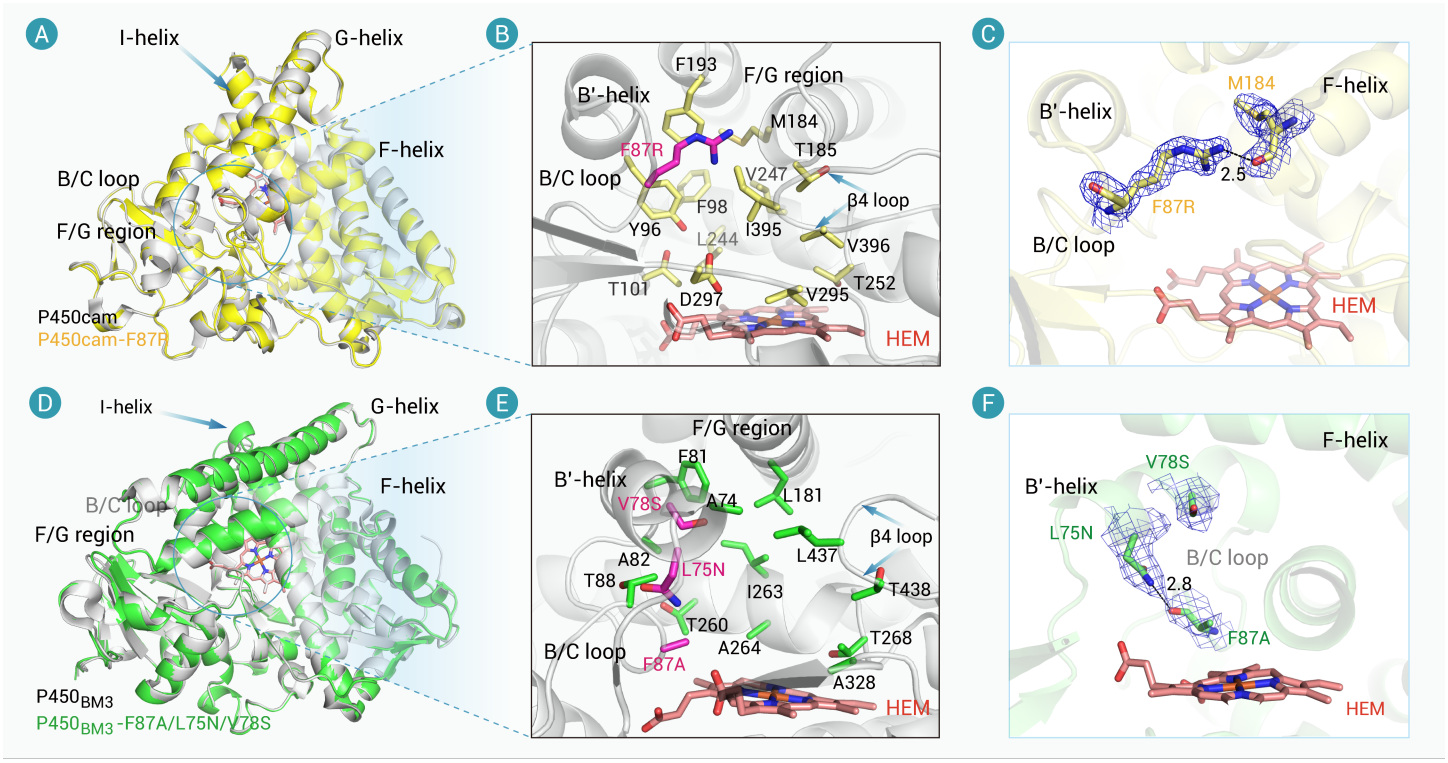

Figure 3. Structural analysis of the substrate-binding pockets in P450 variants (A) Superimposition of the substrate-free structures of P450cam-F87R (yellow, PDB ID: 25BV) with P450cam-WT (gray, PDB ID: 2A1M)[34]. (B) Detailed view of the active pocket of P450cam-F87R, with the surrounding secondary structural elements labeled. (C) Conformational analysis of the mutated residue in P450cam-F87R. (D) Structural overlay of $P450_{BM3}$-F87A/L75N/V78S (green, PDB ID: 9L7U) with the wild-type $P450_{BM3}$ (gray, PDB ID: 1ZO9)[35]. (E) Detailed view of the active pocket of $P450_{BM3}$-F87A/L75N/V78S, with the surrounding secondary structural elements labeled. (F) Conformational analysis of mutated residues in $P450_{BM3}$-F87A/L75N/V78S.

the two (−)-ambroxide 3*β*-hydroxylases investigated herein, site-specific mutations modulate the volume and/or conformational properties of the corresponding amino acid side chains (Figure S13), thereby enlarging the catalytic pocket and reshaping its geometry. These structural changes provide a mechanistic rationale for the accommodation of substrates bearing a tricyclic ring scaffold.

In the catalytic pocket of P450cam-F87R, a distinct substrate density corresponding to the shape of (−)-ambroxide was observed (Figures 4A & S14). The substrate binds to this P450 enzyme variant mainly via hydrophobic interactions. Of note, the F87R mutation leads to a crucial hydrogen bond (~3.1 Å) between the guanidine group and the only heteroatom in the substrate (Figure 4A). This key interaction serves as an anchor, determining the orientation of the substrate within the active pocket. In this complex structure, the *proS*-H at the C-3 position of the substrate was found to be in the closest proximity (4.3 Å) to the heme-iron reactive center (Figure 4B), suggesting the formation of an *S*-configuration product (*i.e.*, 3*β*-OH-ambroxide). A 200-ns molecular dynamics (MD) simulation was performed to assess the stability of the substrate-binding conformation in P450cam-F87R (Figure S15). Throughout the trajectory, the *proS*-H is consistently closer to the oxo atom (O1) of Fe(IV)=O^{2-} (Compound I) compared to the *proR*-H. This observation is consistent with the crystallographic structure and biochemical reaction data.

Similar to P450cam, a significant substrate density was observed in the substrate binding pocket of $P450_{BM3}$-F87A/L75N/V78S, with the ligand (−)-ambroxide well modeled (Figures 4C & S16). The hydroxyl oxygen atom of V78S is positioned 3.0 Å away from the substrate oxygen atom, facilitating substrate anchoring via a hydrogen bond. In this complex, the *proS*-H at the C3 position of the substrate is in closest proximity to the Fe atom of the heme group, at a distance of 3.1 Å (Figure 4D). A 200 ns MD simulation confirmed that the *proS*-H consistently remains closer to the O1 of Compound I compared to the *proR*-H (Figure S17). The above-described biochemical experiments confirmed that the product of this mutant adopts an *S*-stereoisomeric form.

Structural basis for the convergent function of the two P450 mutants

P450cam and $P450_{BM3}$ have long been used as model proteins for investigating catalytic mechanisms and as enzyme templates for engineering new functionalities.[14,17,18] Although these two enzymes process natural substrates with distinct structural types and geometric shapes (cyclic terpene *versus* linear fatty acid), laboratory convergent evolution has enabled the development of variants from both enzymes capable of catalyzing the same reaction of a common substrate (−)-ambroxide, yielding the same product 3*β*-OH-ambroxide. This result suggests that mutating a limited number of residues within distinct catalytic pockets can effectively reshape the catalytic activity and selectivity of P450 enzymes, as seen in F87R in P450cam and F87A/L75N/V78S in $P450_{BM3}$ (Figure 5).

During the convergent evolution of P450cam and $P450_{BM3}$ towards recognizing the tricyclic substrate (−)-ambroxide, both enzymes experienced expansion of their active pockets. In P450cam-WT, the bulky side-chain of F87 initially occupies space above the catalytic pocket, causing significant

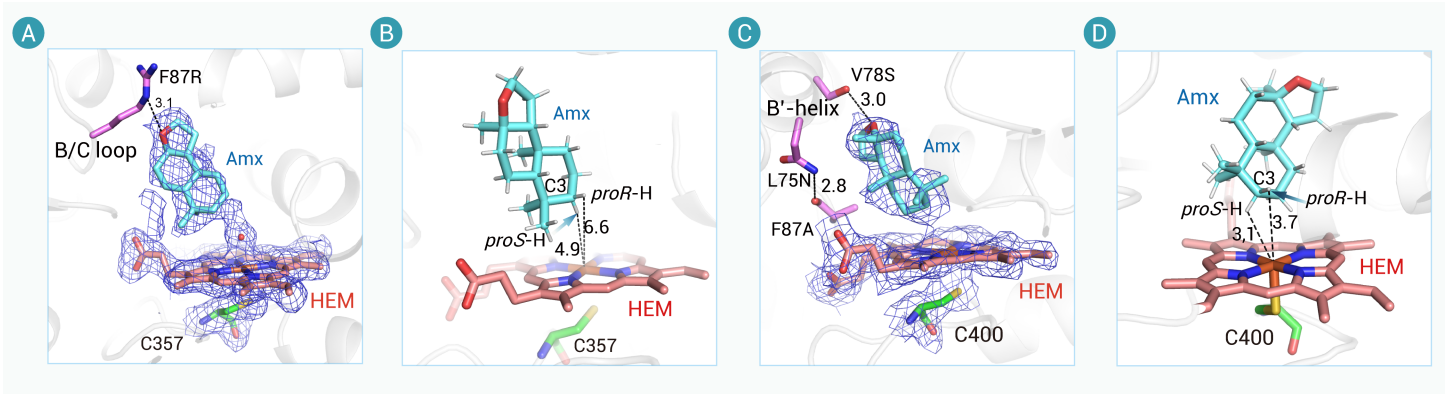

Figure 4. Structural basis for the regio- and stereoselectivity of P450 variants toward (−)-ambroxide (A) Electron density map of (−)-ambroxide in the substrate binding pocket of P450cam-F87R (PDB ID: 9L7R). (B) The distances between the two C−H bonds at the C3 position of the substrate and the heme-iron in the 9L7R structure. (C) Electron density map of (−)-ambroxide in the substrate binding pocket of $P450_{BM3}$-F87A/L75N/V78S. (D) The distances between the two C−H bonds at the C3 position of the substrate and the heme-iron in the 9L7U structure. The $2mF_o$-DF_c densities for the ligand, heme, and residues are outlined in blue at a 1.0 σ level. The distances are indicated in angstroms.

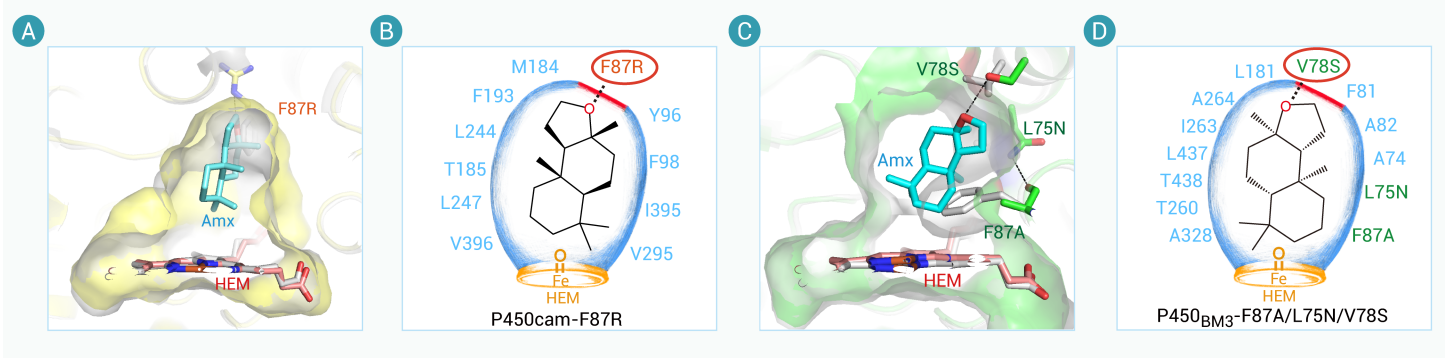

Figure 5. Comparative analysis of the substrate binding pockets of P450 variants (A, C) Cross-sectional structural overlays of the substrate-binding pockets of P450cam-WT and P450cam-F87R (A), and of $P450_{BM3}$ and $P450_{BM3}$-F87A/L75N/V78S (C), presented from the same angle of view. (B, D) Schematic illustrations of the substrate binding modes of (−)-ambroxide in P450cam-F87R (B) and $P450_{BM3}$-F87A/L75N/V78S (D).

steric hindrance with the non-native substrate (−)-ambroxide (Figures 5A-B). Upon mutation to arginine with a similarly large side-chain, R87 forms a hydrogen bond with M184, adopting a compact conformation that results in an expansion of the catalytic pocket volume (Figure 5A). Attempting to replace F87 with tryptophan with an even larger side chain led to a reduced activity towards (−)-ambroxide,[22] further confirming the importance of the volume and shape of the substrate binding pocket in governing the catalytic activity. In the innate $P450_{BM3}$, F87 is located at the end of the substrate access channel directly above the heme group, playing a size-dependent role in modulating the enzyme activity. Substituting this residue with a smaller alanine residue significantly increases the volume available for substrate accommodation (Figure 5C). Additionally, mutations introducing polar amino acids above the catalytic pocket, such as F87R in P450cam and V78S in $P450_{BM3}$, establish hydrogen-bonding interactions with the only oxygen atom in the substrate, thereby stabilizing its conformation via an anchoring mechanism (Figures 5C-D).

Taken together, these mutations reshape the substrate binding pockets of both P450 enzymes, expanding their volume to accommodate the bulky substrate (−)-ambroxide. Additionally, the introduction of different polar amino acids at distinct positions within the active pockets orients the substrate via the specific interaction with the only heteroatom, leading these two evolutionarily distant P450 enzymes to give an identical catalytic outcome (Figures 5C-D). Of note, structural superposition analysis revealed that the common 3β-hydroxylated product should result from distinct substrate binding modes and rotated conformations (Figure S18). Despite these differences, the C3-*proS*-H of (−)-ambroxide is oriented toward the heme-iron center in both cases. Moreover, these mutations all occur on the BB' loop (P450cam-F87), B'-helix ($P450_{BM3}$-V78) or BC loop ($P450_{BM3}$-F87), which are crucial components forming the active pocket and determining the substrate specificity of P450 enzymes,[43,44] highlighting their significance in P450 enzyme engineering.

MD and QM/MM calculations for understanding the regio- and stereoselectivity

To understand the origin of the shared regio- and stereoselectivity of P450cam-F87R and $P450_{BM3}$-F87A/L75N/V78S, we carried out MD simulations and QM/MM calculations. MD analysis showed that, compared with P450cam-WT and $P450_{BM3}$-WT, the substrate in P450cam-F87R and $P450_{BM3}$-F87A/L75N/V78S more frequently adopts conformations with a shorter *proS*-H···O1 distance and a more favorable attack angle, often exceeding 130° (Figures S15 & S17). Based on these geometric parameters, Near Attack Conformation (NAC) density distributions were constructed. Here, donor-acceptor distances < 3.0 Å and attack angles > 130° were defined as catalytically competent for *proS/R*-H atom transfer. Comparisons of the NAC populations between wild-type and mutant enzymes showed that, in the F87R and F87A/L75N/V78S mutant cluster, MD conformations favorable for *proS*-H attack on O1 were substantially enriched (Figures S19-S20). These results indicate that the F87R and F87A/L75N/V78S mutations effectively restrict substrate orientation and thereby promote selective hydroxylation at the *S*-site, giving rise to the major product.

To further understand the shared regio- and stereoselectivity of P450cam-F87R and $P450_{BM3}$-F87A/L75N/V78S, we performed a series of QM/MM calculations. For P450cam-F87R, the substrate-binding conformation positions the C3 site in close proximity to the oxygen atom (O1) of Compound I. MD simulations confirm that the *proS*-H at C3 remains closer to the oxo moiety of Compound I than the *proR*-H throughout the trajectory (Figure S15). A representative conformation extracted from the equilibrated MD trajectory was employed for QM/MM simulations (Figure 6A). The reaction is initiated from the optimized reactant (RC_{F87R}), consisting of Compound I and the substrate. We scanned hydrogen atom transfer (HAT) from either the *proS*-H or *proR*-H at the C3 position by the Fe(IV)=O^{2-} species. For the *proS*-H abstraction pathway, the reaction proceeds with an energy barrier of 18.5 kcal/mol (RC_{F87R}→$TS1_{F87R(S)}$), yielding a Fe(III)-OH^- intermediate ($IC1_{F87R(S)}$) with a relative energy of 12.6 kcal/mol. The subsequent OH

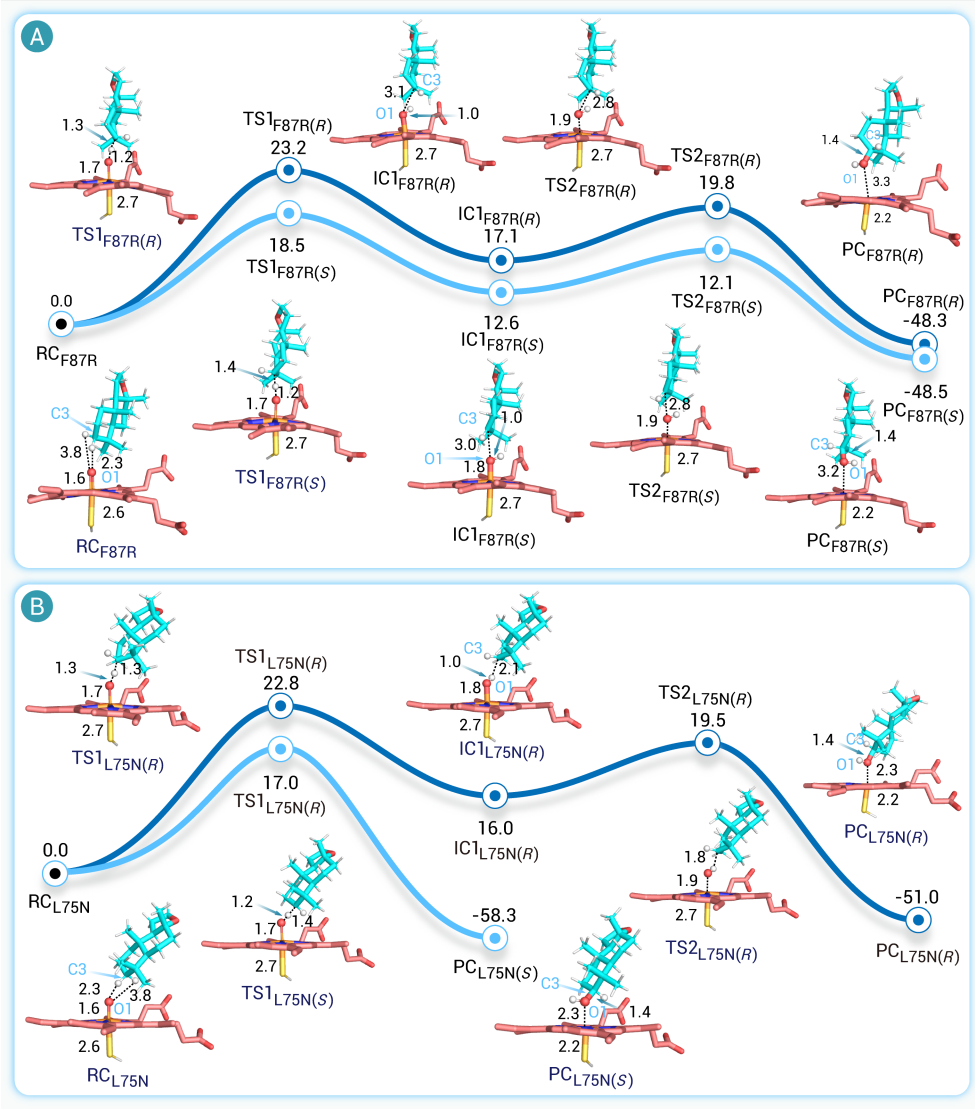

Figure 6. QM/MM-derived mechanisms for the regio- and stereoselective hydroxylation of (−)-ambroxide catalyzed by the two P450 mutants (A) Proposed mechanism for the formation of the *proS*-hydroxylated product catalyzed by P450cam-F87R. (B) Proposed mechanism for the formation of the *proS*-hydroxylated product catalyzed by $P450_{BM3}$-F87A/L75N/V78S. Each panel shows the key steps of hydrogen atom transfer (HAT), Fe(III)−OH^- intermediate formation, and OH radical rebound, along with the QM/MM-optimized structures of representative species. Distances are given in angstroms (Å).

rebound step occurs with a negligible additional barrier, affording the *proS*-hydroxylated product ($PC_{L75N(S)}$) in a highly exothermic process (ΔE = −48.5 kcal/mol). In contrast, *proR*-HAT requires overcoming a higher barrier of 23.2 kcal/mol ($TS1_{F87R(R)}$) and results in an endothermic intermediate ($IC1_{F87R(R)}$, 17.1 kcal/mol), indicating that this pathway is both kinetically and thermodynamically disfavored. These results reveal that P450cam-F87R should exhibit strict stereoselectivity toward *proS*-hydroxylation at the C3 position, as experimentally observed (Figure 2).

For $P450_{BM3}$-F87A/L75N/V78S (hereafter denoted as right subscript $_{L75N}$ in Figure 6B), MD simulation revealed that the *proS*-H at the substrate's C3 position remains closer to the oxo atom of Compound I than the *proR*-H throughout the trajectory (Figure S17). The *proS*-H abstraction proceeds via the $TS1_{L75N(S)}$ (Figure 6B) with a barrier of only 17.0 kcal/mol, followed by a spontaneous OH radical rebound from the Fe(III)−OH^- intermediate, directly yielding the *proS*-hydroxylated product ($PC_{L75N(S)}$). In contrast, *proR*-H abstraction is kinetically less favorable, requiring the overcoming of a 22.8 kcal/mol barrier to form the Fe(III)−OH^- species ($IC1_{L75N(R)}$), which undergoes OH rebound via an energy barrier of 19.5 kcal/mol to afford the *proR*-hydroxylated product ($PC_{L75N(R)}$). It confirms that $P450_{BM3}$-F87A/L75N/V78S favors the formation of the *proS*-hydroxylated product. Due to the detection of a trace amount of the 3-keto-ambroxide by-product, we also evaluated its formation catalyzed by Cpd I and the corresponding thermodynamic requirements (Figures S21-S22). Starting from the major *proS*-hydroxylated product ($IC1_{F87A/L75N/V78S(S)}$, hereafter denoted as $IC1'_{L75N(S)}$), the Cpd I-mediated H-transfer was calculated to require a barrier of 18.3 kcal/mol, with the intermediate $IC2'_{L75N(S)}$ exhibiting a substantial endothermicity of 13.1 kcal/mol. The second H-transfer occurs at the C3−H position and requires an even higher barrier of 21.5 kcal/mol, ultimately yielding the keto product $PC'_{L75N(S)}$. The relatively high reaction barriers confirm that the formation of this by-product is thermodynamically disfavored. The spin density and QM/MM potential energy data for all reactants, transition states, intermediates, and products involved in the above reaction are summarized in Tables S2 & S3.

DISCUSSION

Enzyme convergent evolution highlights the diversity and plasticity of functional evolution, demonstrating that an identical catalytic function can emerge from distinct sequence and structural backgrounds. Studying such isoenzymes could provide fundamental insights into structure-function relationships by revealing the plasticity-determining residues and active-site geometries required for a given reaction. Moreover, these naturally evolved solutions would serve as valuable guides for protein design and engineering. Classic examples include the independent emergence of the Ser−His−Asp catalytic triad in proteases such as chymotrypsin and subtilisin, where a conserved charge-relay mechanism enables peptide bond hydrolysis despite distinct folds, as well as the convergence of structurally diverse superoxide dismutases and cellulases with similar catalytic strategies.[45,46] Analogously, our artificial evolution of P450 enzymes achieves comparable regio- and stereoselective oxidation on a much shorter timescale, underscoring that functional constraints drive convergence toward conserved catalytic geometries regardless of evolutionary origin.

Artificial convergence of enzymes not only generates functionally equivalent solutions across different scaffolds but also allows systematic exploration of functional plasticity and structural diversity, thereby accelerating the identification of optimal biocatalysts for specific applications. In our previous study, we employed the MEMS evolutionary approach to achieve functional convergence of non-homologous P450 enzymes that possess distinct active sites. In the quest to optimally engineer enzymes, it is imperative to resolve the following issues: (i) What are the plasticity-relating residues and active-site geometry required for a given P450 reaction? (ii) Is there any quantifiable characteristic that can be conveniently procured to anticipate the activity of any P450 enzyme? (iii) Which regions in P450s are crucial for governing its selectivity in oxidizing distinct substrates?

Addressing these important questions requires dissecting how the active-site architecture shapes regio- and stereoselectivity. The geometric and electrostatic characteristics of the active site facilitate the selective binding to a specific substrate molecule, thereby conferring a high degree of specificity to the enzyme's catalytic actions.[34] In this study, we have elucidated the mechanisms underlying the regio- and stereoselectivity of P450cam-F87R and $P450_{BM3}$-F87A/L75N/V78S towards a common substrate (−)-ambroxide. The two enzymes possess distinct active-site geometries, but exhibit analogous

polar and hydrophobic interactions. Based on our comparative analysis of the crystal structures, we found that the conformational change of the B' helix at the substrate entrance and the displacement of this helix are critical for reshaping the substrate binding pocket. This reshaping modulates substrate entrance and positions the C–H bond for oxidation by the oxidative species of P450s.

The polar heteroatom, specifically the single oxygen atom in (–)-ambroxide, plays a pivotal role in determining the binding mode through specific substrate-enzyme interactions. This study offers an important example of the strategies for the swift engineering of P450 enzymes. These specific substrate-enzyme interactions are crucial in determining the binding mode and orientation. For instance, $P450_{eryF}$ is responsible for the 6*S*-hydroxylation of 6-deoxyerythronolide B. The C5-OH group of the substrate is involved in a hydrogen bond network that facilitates a proton shuttle pathway during the dioxygen bond cleavage reaction.[47] In future P450 enzyme engineering, the B' helix of P450 could serve as a primary target for mutagenesis to tailor P450 substrate specificity. The anchoring-like interaction between the substrate and the enzyme's active site residue will be further harnessed to improve both catalytic efficiency and selectivity.

The study of isoenzymes arising from convergent evolution holds significant value for biocatalysis and industrial biotechnology. Isoenzymes with identical functions but distinct structural frameworks greatly expand the available enzyme repertoire, enabling the selection of variants with appropriate catalytic efficiency, cofactor preference, and/or subcellular localization. Moreover, isoenzymes could serve as functional substitutes for those enzymes that are difficult to express in industrial chassis, and for providing other desirable properties (*e.g.*, thermostability and organic solvent tolerance) to improve industrial applicability. Comparative analysis of their substrate-enzyme interactions and catalytic mechanisms would provide valuable information for further relevant enzyme engineering.

CONCLUSION

In summary, this work provides significant insights into reshaping the catalytic pocket to control the regio- and stereoselectivity of oxidation reactions in two P450 enzymes with low sequence similarity. Detailed structural analysis of the functionally convergent P450 variants enables the understanding of how distinct active sites can reach a common catalytic goal. More generally, combining pocket geometry modulation with the introduction or optimization of polar residues offers a rational strategy to control substrate positioning/orientating, thereby enhancing catalytic activity as well as regio- and stereoselectivity across diverse P450 and non-P450 oxidative biocatalysts. We envision that these mechanistic insights and understandings will not only benefit the future (semi-)rational design of P450 and non-P450 enzymes, but also inspire other studies on isoenzymes.

REFERENCES

1. Guillemard L., Kaplaneris N., Ackermann L., et al. (2021). Late-stage C–H functionalization offers new opportunities in drug discovery. *Nat. Rev. Chem.* **5**:522–545. DOI:10.1038/s41570-021-00300-6
2. McIntosh J. A., Farwell C. C. and Arnold F. H. (2014). Expanding P450 catalytic reaction space through evolution and engineering. *Curr. Opin. Chem. Biol.* **19**:126–134. DOI:10.1016/j.cbpa.2014.02.001
3. Xu H.-J., Fan Z., Nian B.-B., et al. (2025). Achieving mono-selective palladium(II)-catalysed C–H activation of arenes with protein ligands. *Nat. Catal.* **8**:948–956. DOI:10.1038/s41929-025-01407-5
4. Sener C., Timokhin V. I., Hellinger J., et al. (2025). Pd/C promotes C–H bond activation and oxidation of p-hydroxybenzoate during hydrogenolysis of poplar. *Nat. Commun.* **16**:5259. DOI:10.1038/s41467-025-60270-x
5. Song F., Zheng M., Wang J., et al. (2023). Chemoenzymatic synthesis of C14-functionalized steroids. *Nat. Synth.* **2**:729–739. DOI:10.1038/s44160-023-00280-z
6. Craven E. J., Latham J., Shepherd S. A., et al. (2021). Programmable late-stage C–H bond functionalization enabled by integration of enzymes with chemocatalysis. *Nat. Catal.* **4**:385–394. DOI:10.1038/s41929-021-00603-3
7. Zhang X. and Li S. (2017). Expansion of chemical space for natural products by uncommon P450 reactions. *Nat. Prod. Rep.* **34**:1061–1089. DOI:10.1039/c7np00028f
8. Zhang X., Guo J., Cheng F., et al. (2021). Cytochrome P450 enzymes in fungal natural product biosynthesis. *Nat. Prod. Rep.* **38**:1072–1099. DOI:10.1039/d1np00004g
9. Bernhardt R. (2006). Cytochromes P450 as versatile biocatalysts. *J. Biotechnol.* **124**:128–145. DOI:10.1016/j.jbiotec.2006.01.026
10. Bernhardt R. and Urlacher V. B. (2014). Cytochromes P450 as promising catalysts for biotechnological application: Chances and limitations. *Appl. Microbiol. Biotechnol.* **98**:6185–6203. DOI:10.1007/s00253-014-5767-7
11. Ma L., Sun T., Liu Y., et al. (2023). Enzymatic synthesis of indigo derivatives by tuning P450 BM3 peroxygenases. *Synth. Syst. Biotechnol.* **8**:452–461. DOI:10.1016/j.synbio.2023.06.006
12. Sirim D., Widmann M., Wagner F., et al. (2010). Prediction and analysis of the modular structure of cytochrome P450 monooxygenases. *BMC Struct. Biol.* **10**:34. DOI:10.1186/1472-6807-10-34
13. Hamdane D., Zhang H. and Hollenberg P. (2008). Oxygen activation by cytochrome P450 monooxygenase. *Photosynth. Res.* **98**:657–666. DOI:10.1007/s11120-008-9322-1
14. Whitehouse C. J., Bell S. G. and Wong L. L. (2012). P450(BM3) (CYP102A1): Connecting the dots. *Chem. Soc. Rev.* **41**:1218–1260. DOI:10.1039/c1cs15192d
15. Schlichting I., Berendzen J., Chu K., et al. (2000). The catalytic pathway of cytochrome P450cam at atomic resolution. *Science* **287**:1615–1622. DOI:10.1126/science.287.5458.1615
16. Gunsalus I. C. and Wagner G. C. (1978). Bacterial P-450cam methylene monooxygenase components: Cytochrome m, putidaredoxin, and putidaredoxin reductase. *Methods Enzymol.* **52**:166–188. DOI:10.1016/s0076-6879(78)52019-3
17. Ahalawat N. and Mondal J. (2018). Mapping the substrate recognition pathway in cytochrome P450. *J. Am. Chem. Soc.* **140**:17743–17752. DOI:10.1021/jacs.8b10840
18. Follmer A. H., Mahomed M., Goodin D. B., et al. (2018). Substrate-dependent allosteric regulation in cytochrome P450cam (CYP101A1). *J. Am. Chem. Soc.* **140**:16222–16228. DOI:10.1021/jacs.8b09441
19. Sevrioukova I. F., Poulos T. L. and Churbanova I. Y. (2010). Crystal structure of the putidaredoxin reductase x putidaredoxin electron transfer complex. *J. Biol. Chem.* **285**:13616–13620. DOI:10.1074/jbc.M110.104968
20. Hollingsworth S. A., Batabyal D., Nguyen B. D., et al. (2016). Conformational selectivity in cytochrome P450 redox partner interactions. *Proc. Natl. Acad. Sci. USA* **113**:8723–8728. DOI:10.1073/pnas.1606474113
21. Hudeeek J., Baumruk V., Anzenbacher P., et al. (1998). Catalytically self-sufficient P450 CYP102 (cytochrome P450 BM-3): Resonance Raman spectral characterization of the heme domain and of the holoenzyme. *Biochem. Biophys. Res. Commun.* **243**:811–815. DOI:10.1006/bbrc.1997.8057
22. Ma L., Li F. W., Zhang X. W., et al. (2022). Development of MEMS directed evolution strategy for multiplied throughput and convergent evolution of cytochrome P450 enzymes. *Sci. China Life Sci.* **65**:550–560. DOI:10.1007/s11427-021-1994-1
23. Xue Y. Q., Wilson D., Zhao L. S., et al. (1998). Hydroxylation of macrolactones YC-17 and narbomycin is mediated by the *pikC*-encoded cytochrome P450 in *Streptomyces venezuelae*. *Chem. Biol.* **5**:661–667. DOI:10.1016/S1074-5521(98)90293-9
24. Du L., Dong S., Zhang X. W., et al. (2017). Selective oxidation of aliphatic C–H bonds in alkylphenols by a chemomimetic biocatalytic system. *Proc. Natl. Acad. Sci. USA* **114**:E5129–E5137. DOI:10.1073/pnas.1702317114
25. Boddupalli S. S., Estabrook R. W. and Peterson J. A. (1990). Fatty acid monooxygenation by cytochrome P-450BM-3. *J. Biol. Chem.* **265**: 4233-4239. https://www.jbc.org/article/S0021-9258(19)39552-3/fulltext
26. Poulos T. L., Finzel B. C. and Howard A. J. (1987). High-resolution crystal structure of cytochrome P450cam. *J. Mol. Biol.* **195**:687–700. DOI:10.1016/0022-2836(87)90190-2
27. Guengerich F. P., Martin M. V., Sohl C. D., et al. (2009). Measurement of cytochrome P450 and NADPH-cytochrome P450 reductase. *Nat. Protoc.* **4**:1245–1251. DOI:10.1038/nprot.2009.121
28. Panicco P., Astuti Y., Fantuzzi A., et al. (2008). P450 versus P420: Correlation between cyclic voltammetry and visible absorption spectroscopy of the immobilized heme domain of cytochrome P450 BM3. *J. Phys. Chem. B* **112**:14063–14068. DOI:10.1021/jp8050033
29. Sevrioukova I. F. and Poulos T. L. (2002). Putidaredoxin reductase, a new function for an old protein. *J. Biol. Chem.* **277**:25831–25839. DOI:10.1074/jbc.M201110200
30. Li S., Podust L. M. and Sherman D. H. (2007). Engineering and analysis of a self-sufficient biosynthetic cytochrome P450 PikC fused to the RhFRED reductase domain. *J. Am. Chem. Soc.* **129**:12940–12941. DOI:10.1021/ja075842d
31. Xu Q., Kong H. T., Liu K., et al. (2023). The biosafety level-2 macromolecular crystallography beamline (BL10U2) at the Shanghai Synchrotron Radiation Facility. *Nucl. Sci. Tech.* **34**:202. DOI:10.1007/s41365-023-01350-9
32. Xiao Q., Wu T., Bao K., et al. (2024). Upgrade of crystallography beamline BL19U1 at the Shanghai Synchrotron Radiation Facility. *J. Appl. Crystallogr.* **57**:630–637. DOI:10.1107/S1600576724002188
33. Kabsch W. (2010). Xds. *Acta. Crystallogr. D Biol. Crystallogr.* **66**:125–132. DOI:10.1107/S0907444909047337
34. Nagano S. and Poulos T. L. (2005). Crystallographic study on the dioxygen complex of wild-type and mutant cytochrome P450cam. Implications for the dioxygen activation mechanism. *J. Biol. Chem.* **280**:31659–31663. DOI:10.1074/jbc.M505261200
35. Hegde A., Haines D. C., Bondlela M., et al. (2007). Interactions of substrates at the surface of P450s can greatly enhance substrate potency. *Biochemistry*

46:14010–14017. DOI:10.1021/bi701667m
36. Adams P. D., Afonine P. V., Bunkoczi G., et al. (2010). PHENIX: A comprehensive Python-based system for macromolecular structure solution. *Acta. Crystallogr. D Biol. Crystallogr.* 66:213–221. DOI:10.1107/S0907444909052925
37. Emsley P., Lohkamp B., Scott W. G., et al. (2010). Features and development of Coot. *Acta. Crystallogr. D Biol. Crystallogr.* 66:486–501. DOI:10.1107/S0907444910007493
38. Li S., Ouellet H., Sherman D. H., et al. (2009). Analysis of transient and catalytic desosamine-binding pockets in cytochrome P-450 PikC from *Streptomyces venezuelae*. *J. Biol. Chem.* 284:5723–5730. DOI:10.1074/jbc.M807592200
39. Zhang X., Jiang Y., Chen Q., et al. (2021). H-bonding networks dictate the molecular mechanism of H_2O_2 activation by P450. *ACS Catal.* 11:8774–8785. DOI:10.1021/acscatal.1c02068
40. Chen J., Dong S., Fang W., et al. (2023). Regiodivergent and enantioselective hydroxylation of C–H bonds by synergistic use of protein engineering and exogenous dual-functional small molecules. *Angew. Chem. Int. Ed. Engl.* 62:e202215088. DOI:10.1002/anie.202215088
41. Ma N. N., Chen Z. F., Chen J., et al. (2018). Dual-functional small molecules for generating an efficient cytochrome P450BM3 peroxygenase. *Angew. Chem. Int. Edit.* 57:7628–7633. DOI:10.1002/anie.201801592
42. Kong F. H., Chen J., Qin X. Q., et al. (2022). Evolving a P450BM3 peroxygenase for the production of indigoid dyes from indoles. *Chemcatchem* 14:e202201151. DOI:10.1002/cctc.202201151
43. Fansher D. J., Besna J. N., Fendri A., et al. (2024). Choose your own adventure: A comprehensive database of reactions catalyzed by cytochrome P450 BM3 variants. *ACS Catal.* 14:5560–5592. DOI:10.1021/acscatal.4c00086
44. Hoffmann G., Bonsch K., Greiner-Stoffele T., et al. (2011). Changing the substrate specificity of P450cam towards diphenylmethane by semi-rational enzyme engineering. *Protein Eng. Des. Sel.* 24:439–446. DOI:10.1093/protein/gzq119
45. Ekici O. D., Paetzel M. and Dalbey R. E. (2008). Unconventional serine proteases: Variations on the catalytic Ser/His/Asp triad configuration. *Protein Sci.* 17:2023–2037. DOI:10.1110/ps.035436.108
46. Galperin M. Y. and Koonin E. V. (2012). Divergence and convergence in enzyme evolution. *J. Biol. Chem.* 287:21–28. DOI:10.1074/jbc.R111.241976
47. Cupp-Vickery J. R., Han O., Hutchinson C. R., et al. (1996). Substrate-assisted catalysis in cytochrome P450eryF. *Nat. Struct. Biol.* 3:632–637. DOI:10.1038/nsb0796-632

FUNDING AND ACKNOWLEDGMENTS

This work was supported by the National Key Research and Development Program of China (No. 2025YFA0923200), National Natural Science Foundation of China (32025001 to S.L., 32571464 and 32071266 to L.M., 32171203 to S.D., 22403094 to W.P.), Qingdao New Energy Shandong Laboratory of Strengthening Foundation Plan (QNESL SFP 202302 to Y.F.), Key R&D Program of Shandong Province to L.M. (2025TSGCCZZB0768), the Taishan Scholars Program of Shandong Province and Shandong Provincial Natural Science Foundation to W.P. (tsqn202507079 and ZR2025QB36). We also thank G. Lin, J. Qu, and H. Sui from the State Key laboratory of Microbial Technology at Shandong University for their assistance in HPLC-HRMS and NMR spectroscopy analyses. The funders had no role in study design, data collection and analysis, decision to publish, or preparation of the manuscript.

AUTHOR CONTRIBUTIONS

L.M., Y.F., and S.L. conceived and supervised the study. L.M., S.D., W.P., Y.F., and S.L. wrote the manuscript. L.M., S.D., J.Z., M.L., Y.L., and H.Z. performed the experiments and analyzed the data. W.P. conducted the QM/MM calculations. All authors read and approved the final manuscript. All authors contributed to the manuscript and approved the final version.

DECLARATION OF INTERESTS

The authors declare no competing interests.

DATA AND CODE AVAILABILITY

Data deposition: the associated structures reported in this paper have been deposited in the Protein Data Bank, www.wwpdb.org (PDB IDs: 25BV, 9L7R, and 9L7U).

SUPPLEMENTAL INFORMATION

It can be found online at https://doi.org/10.59717/j.xinn-life.2026.100221.

LEAD CONTACT WEBSITE

Shengying Li (http://eeg.qd.sdu.edu.cn/index.htm)